Journal of Magnetism and Magnetic Materials 383 (2015) 94–99

Contents lists available at ScienceDirect

Journal of Magnetism and Magnetic Materials

journal homepage: www.elsevier.com/locate/jmmm

Conversion of magnetic anisotropy in electrodeposited Co–Ni alloy nanowires

A.S. Samardak [a,*], F. Nasirpouri [b,*], M. Nadi [b], E.V. Sukovatitsina [a], A.V. Ognev [a], L.A. Chebotkevich [a], S.V. Komogortsev [c]

[a] School of Natural Sciences, Far Eastern Federal University, Vladivostok, Russian Federation
[b] Faculty of Materials Engineering, Sahand University of Technology, Tabriz, Iran
[c] Institute of Physics, SB Russian Academy of Sciences, Krasnoyarsk, Russian Federation

ARTICLE INFO

Article history:
Received 8 July 2014
Received in revised form
7 October 2014
Accepted 8 October 2014
Available online 31 October 2014

Keywords:
Coercive force
Magnetic anisotropy
Magnetic hysteresis
Binary alloy nanowires
Alumina template
Electrodeposition

ABSTRACT

In this paper, the influence of alternating current (ac) electrodeposition frequency and waveform is reported on chemical composition, microstructure and consequently magnetic properties of Co–Ni binary alloy nanowire arrays embedded in an alumina template. For sinusoidal and square electrodeposition waveforms the easy axis of magnetization rotates from being parallel to perpendicular orientation to nanowire long axis as the deposition frequency increases from 200 to 800 Hz. The reason for the drastic change of magnetic anisotropy in nanowires is attributed to the increase of cobalt content and the crystal structure phase transformation from *fcc–hcp* mixture at high Ni content to *hcp* at high Co content. We explain the conversion of magnetic behavior of nanowire arrays in terms of a competition between the shape and magnetocrystalline anisotropies.

1. Introduction

MAGNETIC nanowires (NWs) as a major category of nanostructures have attracted great interest for many applications such as electronics, magnetics and devices [1,2]. Compared with physical methods such as nanolithography and other model methods, these nanowires can be readily and effectively synthesized using chemical and electrochemical techniques [3]. Electrochemical deposition is a simple and cheap method to produce NWs. Nanowires with a high length to diameter ratio can be grown into porous membranes such as anodic aluminum oxide (AAO) [4,5].

Template electrodeposition using direct current (dc) is known as a traditional way to fabricate a range of compositions and structures in magnetic NWs. However, it requires the templates to become conductive in a distinct process. In contrast, ac electrodeposition enables direct deposition of NWs into AAO. In this technique, ac current factors including amplitude, frequency and waveform have significant effects on the growth and properties, though; so far little work has been carried out in this field. Magnetic properties and microstructures of magnetic Co nanowires can be controlled by adjusting the deposition parameters [6]. Usually electrodeposition of Co nanowires leads to a polycrystalline structure with wires having many grains with random c-axis orientation [7]. Many works have been done to rotate the *c*-axis of *hcp* Co grains parallel or perpendicular to the nanowire axis [8–11]. As a result, transformation of crystal structure in nanowires changes the magnetic behavior which is driven by the effective magnetic anisotropy K_{eff} depending on competition between the shape and magnetocrystalline anisotropies. One possibility to tune K_{eff} is to produce binary alloy nanowires of cobalt and nickel [12–16]. Nanowires with tailored crystal structures can be produced by variation of electrodeposition conditions mainly through an adjusting of bath pH and/or temperature, amplitude of electroplating current, aspect ratio of template pores, amplitude and orientation of an external magnetic field during electrodeposition [11,17–19]. A little attention has been paid to tune the crystal structure of nanowires by variation of frequency and waveform of electrodeposition current. This paper aims to understand the magnetic behavior of cobalt-based binary nanowires by the addition of nickel as an alloying element controlled by ac parameters.

2. Experimental

Co–Ni NWs were produced by ac electrodeposition into AAO template. We used two-step anodization technique to prepare

* Corresponding authors.
E-mail addresses: samardak.as@dvfu.ru (A.S. Samardak), nasirpouri@sut.ac.ir (F. Nasirpouri).

http://dx.doi.org/10.1016/j.jmmm.2014.10.047
0304-8853/

AAO as completely described in [4,5]. Anodization was conducted for 6 h at each step at 40 V in 0.3 M oxalic acid. In order to modify AAO templates, the thickness of the barrier layer at the bottom of the pores was decreased by step-wise reduction of the anodizing voltage at the end of the second stage of anodization. Electrodeposition bath containing 28 g/l $CoSO_4 \cdot 7H_2O$, 72 g/l $NiSO_4 \cdot 6H_2O$ and 30 g/l H_3BO_3 was prepared by dissolving reagent grade chemicals in deionized water. Ac electrodeposition under constant voltage amplitude was conducted. Two-electrode electrodeposition cell was used consisting of an ac function generator as the power source connected to computer through an A/D data acquisition card to apply and control a range of deposition frequency from 200 to 800 Hz, voltage amplitude (18 V) and waveforms (sinusoidal and square). Voltage amplitude was maintained constant under the conditions of this study as the four stage of growth of NWs in AAO template could be readily achieved.

Transmission electron microscopy (TEM ARM200F, JEOL), scanning electron microscopy (SEM Supra, Carl Zeiss), X-ray diffraction (XRD-Brucker, using the incident Cu Kα radiation (1.54 Å)) technique, energy dispersive X-ray analysis (EDX Oxford Inst.) and atomic force microscopy (Ntegra Aura, NT-MDT) were used to examine the morphology and structure of electrodeposited NWs. Magnetic properties of Co–Ni NWs were defined according to magnetization curves measured using the highly sensitive home-made vibrating sample magnetometer (VSM) in magnetic field range ± 3 kOe. Integral magnetization measurements were carried out at room temperature. The magnetic hysteresis loops were measured by rotation of samples with a step of 10° with respect to the direction of the applied field in the interval of 0–360°. The external magnetic field was applied in-plane of the alumina template and rotated toward the perpendicular to the plane direction with a step of 10° (NWs axis is perpendicular to the plane of the template). From the hysteresis loops we determined the normalized remanence M_r/M_s (where M_r is remanent magnetization at zero field, M_s is saturation magnetization) and coercive force H_c.

3. Results and discussion

3.1. Composition and microstructure

Co–Ni nanowires were electrodeposited into AAO templates with an average pore diameter of 40 ± 2 nm and length of 4 ± 0.2 μm and an interpore distance (from center to center) of 100 ± 4 nm. Size distribution histograms of AAO templates were obtained on SEM images. A typical SEM image of AAO template consisting of top and cross-sectional views is shown in Fig. 1. SEM shows that NW arrays have near hexagonal distribution of pores on short-range order only. The areas with hexagonal arrangement are disoriented in respect to each other. The formation of such arrangement has been precisely described in previous reports [4,5] for estimation of areas of highly ordered regions.

TEM microscopy (Fig. 2a) on isolated NWs confirmed the diameter and quality of nanowires. Using electron energy-loss spectrometry (EELS) with atomic-level chemical analysis resolution, the uniformity of atomic-levels distribution of both Co and Ni was observed on EELS maps confirming the formation of Co–Ni binary alloy instead of Co and Ni segregated phases, Fig. 2b. Selected area electron diffraction (SAED) revealed that crystal structure of NWs has a preferred plane orientation (texture) in dependence on the Co–Ni alloy composition. SAED pattern for NWs electrodeposited at $f=800$ Hz shows hexagonal symmetry (inset in Fig. 2a), indicating that wires are polycrystalline with *hcp*-phase texture having *c*-axis perpendicular to the wire long axis. SAED patterns of other samples also reveal that electrodeposition at lower frequencies leads to polycrystalline NWs with *fcc–hcp* phase mixture.

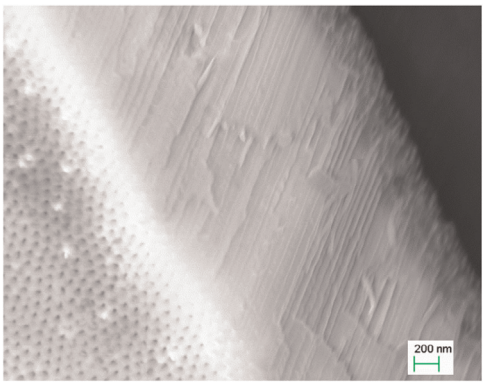

Fig. 1. SEM image of the porous AAO template with the cross-sectional view of pores filled with Co–Ni NWs at 18 V, 800 Hz, sinusoidal waveform.

Fig. 3 illustrates XRD patterns of NW arrays taken while they are embedded in AAO templates. The characteristics of nickel and cobalt diffraction peaks significantly depend upon the change of electrodeposition frequency and waveform. Peaks corresponding to planes of cobalt and nickel are listed in Table 1. The formation of polycrystalline Co-*hcp* showing a texture along the [100] and [002] directions is observed for all the samples. This will have a strong effect on magnetocrystalline anisotropy. Generally, a Bragg diffraction peak appeared at about 44.7° corresponds to different crystalline scatterings coming from our complicated samples including Co (111)-*fcc*, or Ni (111)-*fcc*, Al (002) and also Co (002)-*hcp*, overlapped on each other which individually could not be easily distinguished here. However, the existence of other diffraction peaks helps one understand the crystalline phase evolution in the NW arrays. Bragg peaks related to Ni (111), Ni (220) and Co(220) indices indicate that Co–Ni crystals have also been formed under different electrodeposition conditions in *fcc* phase. It is worth mentioning that Al also contributes to 002, 022 and 103 indices not indicated on the graph coming from aluminum substrate. With decreasing of deposition frequency, the intensity of Co(100)-*hcp* peak is rising for both waveforms indicating that *hcp* phase is dominantly formed. At 800 Hz applied under the square signal, the peak (100) of *hcp*-Co disappears, but intensity of *fcc* Co–Ni peaks do not change. We explain this fact by overlapping of *fcc* Co–Ni peaks with Al, whose contribution to peak intensity does not change from sample to sample. XRD results show a major change of crystalline structure from *fcc–hcp* to *hcp* phase in Co–Ni alloy nanowires with decreasing of the electrodeposition frequency. It is worth noting that the presence of Al peaks may mislead the precise interpretation of phase evolution with frequency change.

The composition of NWs was extracted from energy dispersive spectra (EDS) and summarized in Table 2. It is generally known that EDS could be used to analyze the chemical composition of metals and alloys, while the accuracy of the composition is highly dependent on many instrumental and experimental conditions on the atomic weight percentage level. We observe a significant change in the chemical composition of the alloy system and therefore, EDS could satisfactorily be used to evaluate the properties. Composition of Co–Ni NWs is very sensitive to the electrodeposition parameters. Nickel and cobalt content depends on electrodeposition waveform. Co content increases for both waveforms. For higher electrodeposition frequencies, i.e. 800 Hz, alloys become richer in cobalt.

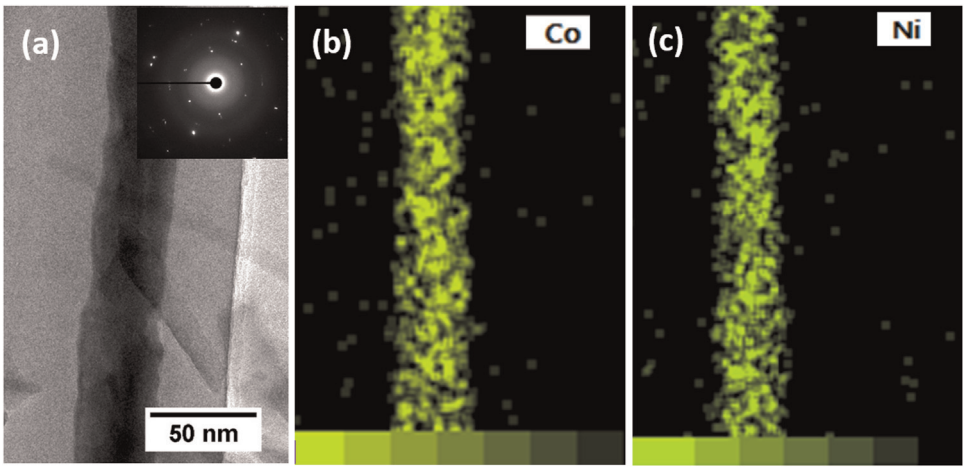

Fig. 2. (a) Dark field TEM image of $Co_{81}Ni_{19}$ NW electrodeposited at sinusoidal waveform with frequency 800 Hz. The inset consists of a spot microdiffraction pattern of a selected area of the same NW. (b) Atomic level EELS maps of Co (b) and Ni (c) atoms in the same NW. The gradient color scale illustrates the relative electron energy loss.

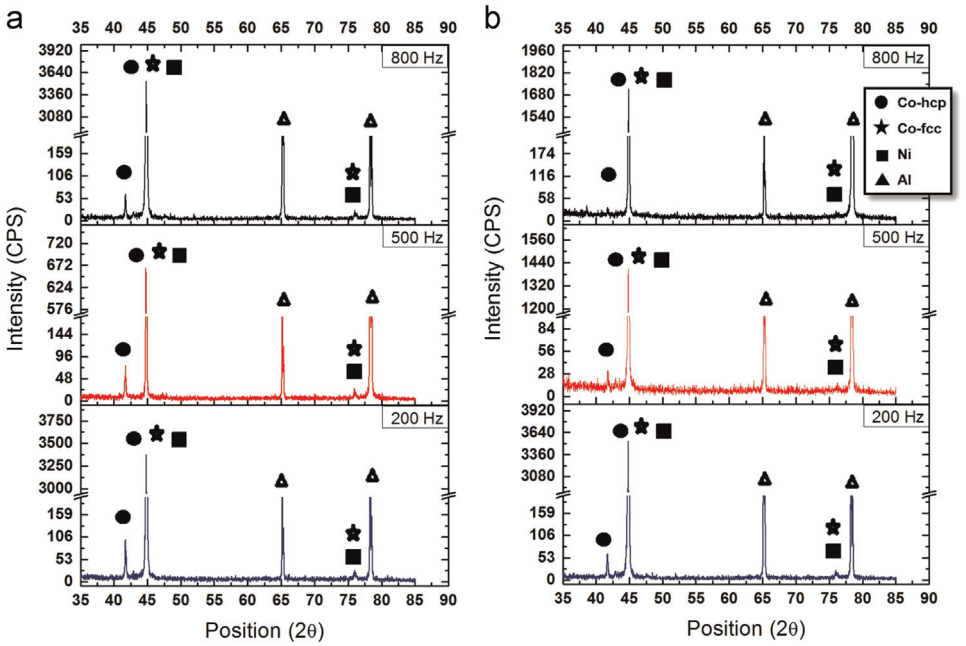

Fig. 3. X-ray diffraction spectra obtained for Co–Ni NWs electrodeposited at 18 V, frequency of 200, 500 and 800 Hz using (a) sinusoidal and (b) square waveforms. Main Bragg peaks for Co and Ni and the estimated Al peaks are labeled by symbols indicated in the inset.

Table 1
Analysis of peaks observed for Co and Ni in XRD patterns for Co–Ni NW arrays electrodeposited in AAO.

Phase	Co-hcp	Co-fcc	Co-fcc	Ni	Ni
2θ (deg)	41.3	44.7	76.1	44.7	76.1
Index	(100)	(002)	(220)	(111)	(220)

Table 2
Composition of Co–Ni NW arrays electrodeposited in AAO under different conditions.

	Sinusoidal signal			Square signal		
Frequency, Hz	200	500	800	200	500	800
Co, at%	68.85	69.06	81.01	65.26	69.64	85.09
Ni, at%	31.15	30.94	18.99	34.74	30.36	14.91

3.2. Magnetic properties

Using the magnetization curves, the polar diagrams of H_c and M_r/M_s measured in the in-plane configuration were plotted. According to these diagrams, no particular anisotropic magnetic behavior inside the arrays was obtained. Magnetic data for the in-plane configuration are listed in Table 3. For both electrodeposition waveforms, coercivity H_c rises significantly when the deposition frequency increases. It can be linked to the mechanism of nucleation and growth during electrodeposition where the composition of NWs becomes richer in cobalt and therefore it increases the coercivity.

Once the magnetization direction changes to out of plane configuration, an anisotropic behavior of the magnetization reversal in NWs is realized. There are examples of the magnetic hysteresis loops measured using VSM when the magnetic field was

applied out of sample plane and rotated in respect of the wire long axis, Fig. 4. In case of out-of-plane rotation the easy axis declines from the parallel to perpendicular to the wire axis with increasing of electrodeposition frequencies.

Figs. 5 and 6 show the dependence of the magnetic properties of NWs on ac electrodeposition frequency. In these figures the polar diagrams of H_c and M_r/M_s at out-of-plane measurement configurations are presented. The behavior of M_r/M_s in dependence on an angle θ between an applied magnetic field and the wire long axis enables one to visualize the direction of easy magnetization axis, indicated by arrows in Figs. 5 and 6. If to combine microstructure data with magnetic properties study, we can conclude that easy axis of magnetization matches *c*-axis of Co-*hcp* lattice in the samples deposited at 800 Hz only.

Table 4 describe magnetic properties of NWs embedded in AAO templates at the out of plane measurement configuration with respect to the easy axis (e.a.) of magnetization.

Our study reveals that with frequency increase for case of sinusoidal and square waveform signals, magnetization easy axis rotates from parallel to perpendicular orientation to the wire axis with respect to *c*-axis of *hcp* phase of Co. As shown above with increase of deposition frequency the composition of Co–Ni alloy changes, Table 1. Consequently, it leads to change of phase from *fcc*–*hcp* mixture at $f=200$ Hz to *hcp* at $f=800$ Hz. This transformation occurs in accordance with the phase diagram for bulk Co–Ni alloy [20].

Table 3
In-plane magnetic properties of Co–Ni NW arrays electrodeposited in AAO under different conditions.

	Sinusoidal signal			Square signal		
Frequency, Hz	200	500	800	200	500	800
H_c, Oe	530	675	760	540	640	875
M_r/M_s	0.48	0.53	0.5	0.37	0.47	0.58

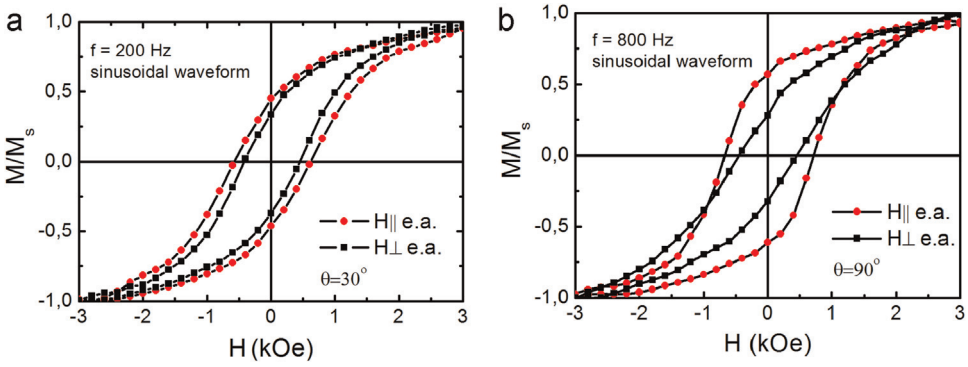

Fig.4. Magnetic hysteresis loops for Co–Ni NWs electrodeposited at different frequencies.

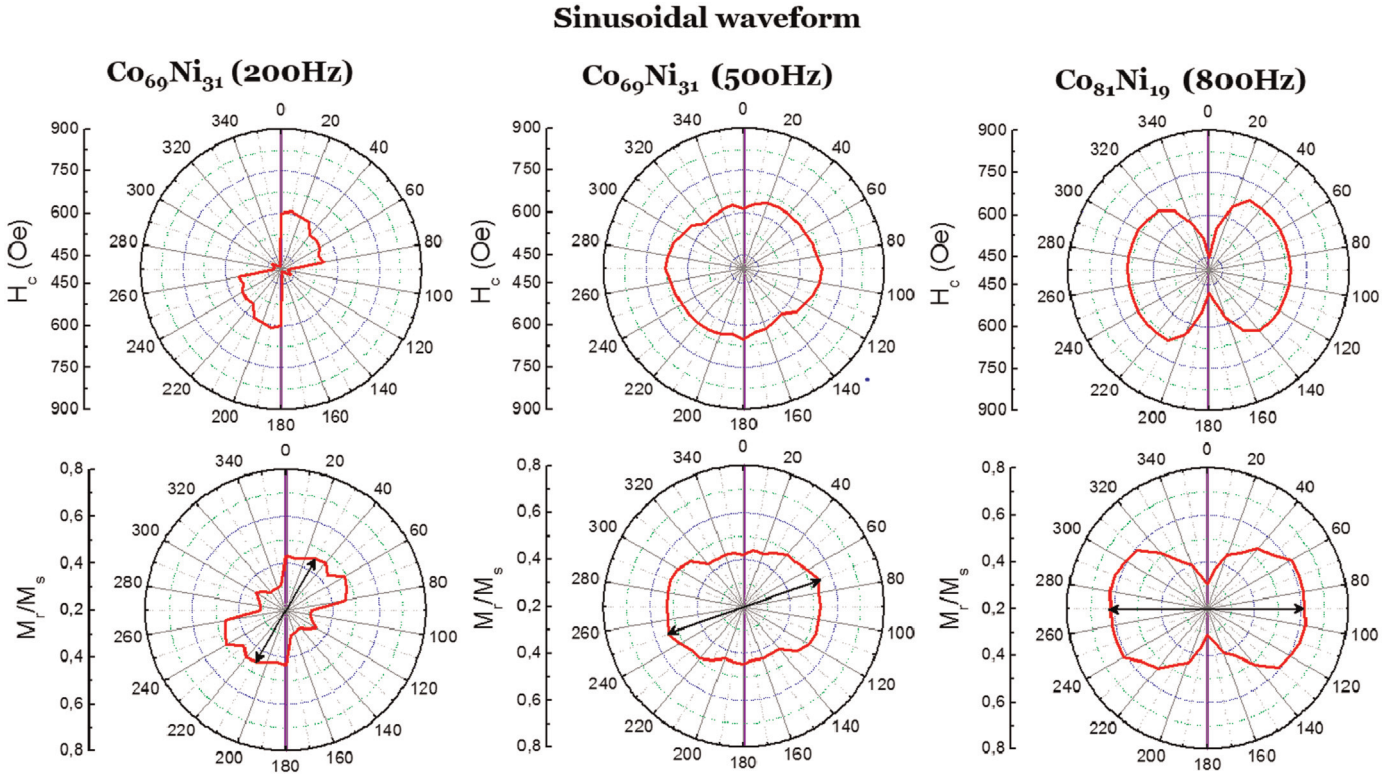

Fig. 5. Polar diagrams of H_c and M_r/M_s for NWs electrodeposited using sinusoidal signal at different frequencies. Zero and 180° angles correspond to the magnetic field alignment parallel to the wire axis. Arrows roughly indicate the easy axis of magnetization.

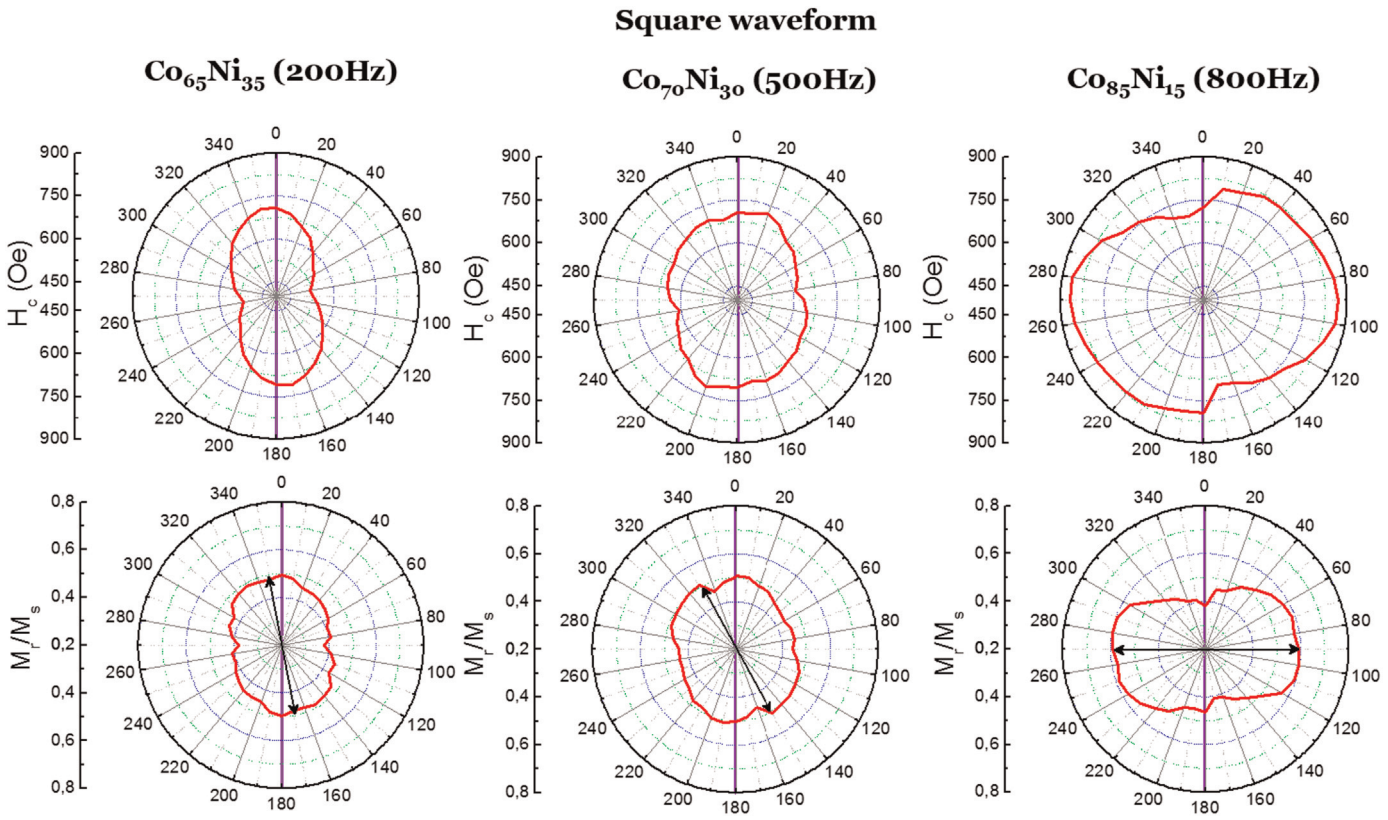

Fig. 6. Polar diagrams of H_c and M_r/M_s for NWs electrodeposited using square signal at different frequencies. Zero and 180° angles correspond to the magnetic field alignment parallel to the wire axis. Arrows roughly indicate the easy axis of magnetization.

Table 4
Out of plane magnetic properties of Co–Ni NW arrays electrodeposited in AAO under different conditions.

	Sinusoidal signal			Square signal		
Frequency, Hz	200	500	800	200	500	800
H_c, Oe (H‖e.a.)	600	670	685	720	680	860
M_r/M_s (H‖e.a.)	0.47	0.55	0.63	0.5	0.52	0.61
H_c, Oe (H⊥e.a.)	425	595	475	535	600	680
M_r/M_s (H⊥e.a.)	0.35	0.43	0.3	0.38	0.46	0.39

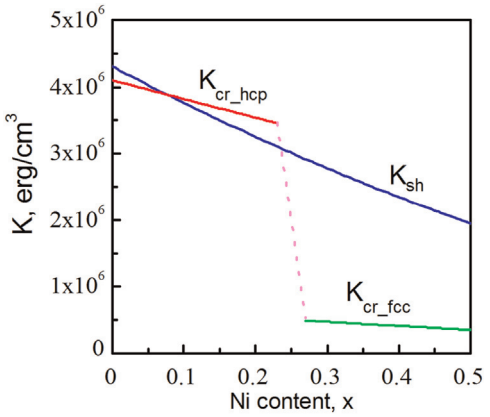

Fig. 7. Dependence of magnetic anisotropies on Ni content in Co–Ni alloy. (For interpretation of the references to color in this figure the reader is referred to the web version of this article.)

The microdiffraction image shown in the inset of Fig. 2a is similar to the diffraction pattern for a single crystal Co nanowire with *hcp* structure and perpendicular to the wire *c*-axis [21,22]. Authors claimed that easy axis of magnetization was aligned perpendicular to the wire long axis due to the competition between magnetocrystalline anisotropy K_{cr} and shape anisotropy K_{sh}, where $K_{cr} > K_{sh}$ at low temperatures only. Actually, at room temperature the constant of crystallographic anisotropy of bulk Co with *hcp* phase is $K_{cr\_hcp}=4.1\times10^6$ erg/cm^3, which is smaller than $K_{sh}=\pi M_s^2=6.2\times10^6$ erg/cm^3 for an individual Co nanowire. It has to lead at normal conditions to the easy axis of magnetization aligned along the wire axis. However, in our case we have worked with the array of binary alloy nanowires, where magnetization depends on its composition and dipole–dipole interaction between NWs. Consequently, shape anisotropy depends on magnetostatic coupling and changes with the content of Co–Ni alloy. It means that K_{sh} can be significantly smaller than K_{cr}.

In Fig. 7 the dependence of K_{sh} (blue bold line) for $Co_{1-x}Ni_x$ alloy is presented. This dependence was calculated as $K_{sh}=\pi(M_s(\mathrm{Ni})x+M_s(\mathrm{Co})(1-x))^2(1-3p)$, where $M_s(\mathrm{Ni})=500$ Gs, $M_s(\mathrm{Co})=1400$ Gs, x is the Ni content in a Co–Ni nanowire and p is the porosity of membrane. The factor $(1-3p)$ takes in to account the dipole–dipole interaction between wires and it was estimated from SEM images of membrane surface [23]. The behavior of magnetocrystalline anisotropy was defined in accordance with the phase diagram of Co–Ni binary alloy [20]. According to this diagram, if the Ni content is below 25 at%, then *hcp* phase is dominant. At the Ni content higher than 27 at%, *fcc* phase is prevalent. The equilibrium mixture of *hcp* and *fcc* is realized at the Ni content lying between 25 and 27 at%. The red line in Fig. 7 indicates K_{cr_hcp}, which correspond to *hcp* phase of Co. At the Ni content higher than 27 at%, Co–Ni alloy has *fcc* structure associated with significantly smaller magnetocrystalline anisotropy marked as K_{cr_fcc} in Fig. 7. As our previous study showed that for pure Co and Co–Ni alloy NWs with the very low Ni content ($x<0.07$) the easy axis of

magnetization aligned along the wire axis. A case, when the easy axis of magnetization aligned perpendicular to the wire long axis, corresponds to a region, where $K_{sh} < K_{cr\_hcp}$. As seen from Fig. 7, this case is realized for the low Ni content ($0.07 < x < 0.24$) in accordance with observed behavior of the easy axis. In alloys with $x > 0.24$ $K_{sh} > K_{cr\_fcc}$ and the easy axis tends to diverge from being perpendicular to the wire direction and finally to be along the wire axis at higher Ni content [24]. This also agrees well with the data of Figs. 5 and 6.

4. Conclusions

Electrodeposition frequency variation leads to change of atomic percentage of Co and Ni. Rising in the frequency assists to increase of Co content. The crystal structure changes from *fcc–hcp* mixture to *hcp* phase with increase of Co percentage. Simultaneously easy axis of magnetization rotates from the being parallel to the perpendicular direction to nanowire long axis. This is discussed as result of the competition between the magnetocrystalline anisotropy of *hcp* crystallites, formed with *c*-axes being perpendicular to the wire axis, and the shape magnetic anisotropy of the Co–Ni nanowire. The value of coercive force is sensitive to the electrodeposition signal waveform. Our results open up a way for tuning electrodeposition of binary alloy nanowires using frequency and waveform manipulation of ac current.

Acknowledgments

This work was supported in part by the Russian Ministry of Education and Science and Far Eastern Federal University. M.N acknowledges the student financial support of Iranian Nanotechnology Initiative Council.

References

[1] A. Huczko, Template-based synthesis of nanomaterials, Appl. Phys. A 70 (2000) 365–376.
[2] D. Yajie, L. Yadong, "Synthesis, assembly and device of 1-dimentional nanostructures", Chin. Sci. Bull 47 (14) (2002) 1149–1156.
[3] M. Hernandez-Velez, "Nanowires and 1D arrays fabrication: an overview", Thin Solid Films 495 (2006) 51–63.
[4] F. Nasirpouri, S.M. Peighambari, "Roughness evolution of highly ordered nanoporous anodic aluminum oxide films", Ionics 19 (2013) 535–542.
[5] F. Nasirpouri, M. Abdollahzadeh, N. Parvini, M. Almasi, "A comparison between self-ordering of nanopores in highly ordered aluminium oxide achieved by two and three step anodic oxidation", Curr. Appl. Phys. 9S (2009) 91.
[6] A. Ramazani, M. Almasi Kashi, M. Alikhani, S. Erfanifam, "Optimized microstructure and magnetic properties in arrays of ac electrodeposited Co nanowires induced by the continuous and pulse electrodeposition", J. Phys. D: Appl. Phys. 40 (2007) 5533–5536.
[7] H. Zeng, M. Zheng, R. Skomski, D.J. Sellmyer, Yi Liu, L. Menon, S. Bandyopadhyay, , "Magnetic properties of self-assembled Co nanowires of varying length and diameter", J. Appl. Phys. 87 (2000) 4718–4720.
[8] Y. Henry, K. Ounadjela, L. Piraux, S. Dubois, J.-M. George, J.-L. Duvail, "Magnetic anisotropy and domain patterns in electrodeposited cobalt nanowires", Eur. Phys. J. B 20 (2001) 35–54.
[9] M. Darques, A. Encinas, L. Vila, L. Piraux, "Tailoring of the c-axis orientation and magnetic anisotropy in electrodeposited Co nanowires", J. Phys.: Condens. Matter 16 (2004) S2279.
[10] J.X. Han, Q. Liu, J. Wang, S. Li, Y. Ren, R. Liu, F. Li, "Influence of crystal orientation on magnetic properties of hcp Co nanowire arrays", Phys. D: Appl. Phys. 42 (2009) 095005.
[11] L.G. Vivas, J. Escrig, D.G. Trabada, G.A. Badini-Confalonieri, M. Vázquez, "Magnetic anisotropy in ordered textured Co nanowires", Appl. Phys. Lett. 100 (2012) 252405.
[12] W.O. Rosan, L.G. Vivas, K.R. Pirota, A. Asenjo, M. Vazquez, "Influence of aspect ratio and anisotropy distribution in ordered CoNi nanowire arrays", J. Magn. Magn. Mater. 324 (2012) 3679–3682.
[13] A. Pereira, C. Gallardo, A.P. Espejo, J. Briones, L.G. Vivas, M. Vázquez, J. C. Denardin, J. Escrig, "Tailoring the magnetic properties of ordered 50 nm diameter CoNi nanowire arrays", J. Nanopart. Res. 14 (2013) 2041.
[14] L.G. Vivas, M. Vazquez, J. Escrig, S. Allende, D. Altbir, D.C. Leitao, J.P. Araujo, "Magnetic anisotropy in CoNi nanowire arrays: analytical calculations and experiments", Phys. Rev. B 85 (2012) 035439.
[15] R.S. Iskhakov, S.V. Komogortsev, L.A. Chekanova, A.D. Balaev, V.A. Yuzova, O. V. Semenova, "The magnetic structure of ferromagnetic filaments of a CoNi (P) alloy in a porous silicon matrix,", Tech. Phys. Lett. 29 (4) (2003) 263–266.
[16] V. Vega, T. Böhnert, S. Martens, M. Waleczek, J.M. Montero-Moreno, D. Görlitz, V.M. Prida, K. Nielsch, "Tuning the magnetic anisotropy of Co–Ni nanowires: comparison between single nanowires and nanowire arrays in hard-anodic aluminum oxide membranes", Nanotechnology 23 (2012) 465709.
[17] D. Kaur, D.K. Pandya, S. Chaudhary, "Texture changes in electrodeposited cobalt nanowires with bath temperature", J. Electrochem. Soc. 159 (2012) D713–D716.
[18] K.R. Pirota, "Magnetic and structural properties of fcc/hcp bi-crystalline multilayer Co nanowire arrays prepared by controlled electroplating", J. Appl. Phys. 109 (2011) 083919.
[19] S. Thongmee, H.L. Pang, J.B. Yi, J. Ding, J.Y. Lin, L.H. Van, "Unique nanostructures in NiCo alloy nanowires", Acta. Mater. 57 (2009) 2482–2487.
[20] Nickel, Cobalt, and Their Alloys (Asm Specialty Handbook). Ed.: Joseph R. Davis, ASM International; Upd Sub edition (January 15, 2001) 425 p.
[21] V. Langlais, S. Arrii, L. Pontonnier, G. Tourillon, "Relationship between structural and magnetic properties of nanosized objects,", Scr. Mater. 44 (2001) 1315–1319.
[22] H.N. Hu, H.Y. Chen, S.Y. Yu, J.L. Chen, G.H. Wu, F.B. Meng, J.P. Qu, Y.X. Li, H. Zhu, John Q. Xiao, "Textured Co nanowire arrays with controlled magnetization direction", J. Magn. Magn. Mater. 295 (2005) 257–262.
[23] V. Vega, V.M. Prida, J.A. García, M. Vazquez, "Torque magnetometry analysis of magnetic anisotropy distribution in Ni nanowire arrays", Phys. Status Solidi A 208 (2011) 553.
[24] E.V. Sukovatitsina, A.S. Samardak, A.V. Ognev, L.A. Chebotkevich, R. Mahmoodi, S.M. Peighambari, M.G. Hosseini, F. Nasirpouri, "Magnetic properties of nickel nanowire arrays patterned by template electrodeposition", Solid State Phenom. 190 (2012) 522.